Hindawi
Advances in Civil Engineering
Volume 2022, Article ID 2044561, 12 pages
https://doi.org/10.1155/2022/2044561

Research Article

Stability Evaluation of Proppant in Fractures of Gas Storage in Yulin Gas Field

Ping Wang,[1] TianLi Gu,[1] Zhanwu Gao,[2] Jiayong Fan,[1] Hai Huang,[1] Zhan Qu,[1] Qiang Han,[1] and Zongxiao Ren[1]

[1]*Xi'an Shiyou University, Xi'an, China*
[2]*PetroChina Changqing Oilfield Company, Xi'an, China*

Correspondence should be addressed to TianLi Gu; 20212010062@stumail.xsyu.edu.cn

Received 9 March 2022; Revised 15 April 2022; Accepted 19 April 2022; Published 28 May 2022

Academic Editor: Xianze Cui

In nearly a hundred years of construction, underground gas storage has become the main natural gas storage and peak regulation means in the world. For the gas storage, the large production and high flow rate of the gas well in the actual production process will cause the backflow of proppant filled in the supporting fracture, which will bring great harm to the gas field production. In this article, when the proppant fracture reaches a stable state in the process of gas injection and production, the stress of proppant particles is analyzed, the critical velocity of proppant reflux is calculated, and then the critical production model is established; calculate the permeability change during proppant migration, then calculate the fluid velocity and production, and determine the fluid velocity range of injection and production wells in gas storage. The parameter sensitivity of velocity and flow model is analyzed. The results show that with the increase of closure stress, the critical gas flow and critical gas velocity of proppant backflow gradually increase, and the proppant filling layer is more stable. The smaller the thickness and width of the filling layer, the greater the critical gas flow and critical gas velocity of proppant backflow, the more stable the proppant filling layer, and the lesser the chance of backflow. The higher the saturation, the lower the critical gas velocity, and the more prone the proppant to reflux. It has important guiding significance for realizing the optimization of gas well production and maintaining efficient production efficiency.

1. Introduction

During the gas injection and production process of the gas storage, the reservoir pressure changes rapidly and sharply, and the proppant in a stable state rolls and is brought into the wellbore, which causes the migration of particles in the reservoir and leads to sand production. The production experience of injection-production wells in gas storage shows that sand production will not only cause permanent damage to the reservoir but also cause erosion damage to the tubing. Due to the lack of data on proppant migration and backflow in gas storage, quite a number of scholars at home and abroad have studied sand production in gas well production and proppant backflow during fracturing, which can provide some ideas and inspiration for our research.

As early as 1970, Hall proposed the concept of "sand arch" for the problem of loose sand production [1]. Based on this theory, Bratli, Milton Taylor, Gidley, Bybee, Karen, Romero, and Feraud [2–6] believed that proppant particles would also form a hemispherical "support arch," and proppant settlement would form in the packing zone. The early stages of stabilizing the structure lead to the formation of small irregular channels on the top and interior of the crack. As the fluid velocity in the fracture increases, the free grains outside the pack continue to erode the sand body until backflow occurs. The instability of sand arch and the erosion of proppant particles were observed through experimental study, and the critical flow rate was determined. Javier, Tooseh [7, 8] established a theoretical model. When the flow rate is steadily increased until a certain point is reached, the proppant particles no longer remain stationary, but "fluidize" under the action of the fluid flow or moisture stream. Taking gas storages in low permeability aquifers as objects, experiments on gas-water-rock interaction and factors

affecting gas storage capacity were carried out. When the original conditions of the reservoir (pH value, temperature, pressure, etc.) remain unchanged, the reservoir is in a stable state. However, when the pH value of the reservoir fluid changes or the flow rate is too fast, its stable state is destroyed, and it is easy to cause acid sensitivity and particle migration in the reservoir [9–13].

Domestic Aspects. Li et al. [14–17] conducted a mechanical analysis of the proppant in gas well production and derived the latest wellbore critical sand-carrying formula that conforms to the actual situation of gas wells. A new formula for the critical production rate of fracture sand production is deduced by proppant stress analysis. Assuming that the proppant accumulates in the fracturing fracture, the relationship between the critical sand production and the bottom hole flow pressure when the gas well fracture is damaged is obtained. Based on the stability similarity and force balance principle between proppant arch and sand arch, Fu and Liu [18, 19] systematically studied the mechanism of proppant backflow during the production process of fracturing gas wells, established a mathematical model of proppant backflow mechanics, and wrote a software for predicting proppant backflow during gas well production. Jin et al. [20, 21] used proppant combinations of different particle sizes to fill fractures to maintain high fracture conductivity. A mathematical model of the movement characteristics of proppant in fractures during fracturing fluid flowback after fracturing is established to simulate the flowback process of fracturing fluid and proppant in fractures when proppant sizes of different particle sizes are combined. Kang [22] conducted an experimental simulation of particle migration caused by rapid changes in gas injection pressure in gas storage wells and revealed the mechanism of particle migration caused by dynamic changes in gas injection pressure in gas storage wells.

As the flow rate increases, the resistance increases. When the flow rate reaches a certain value, the proppant no longer maintains a mechanical equilibrium state and is carried and moved by the fluid, resulting in the backflow of the proppant in the gas well. In this article, the force analysis of proppant in artificial fractures under injection and production conditions is carried out, the prediction model of proppant backflow under high-strength injection and production conditions is established, the critical flow rate is determined, the critical production model is established, and the stability of proppant in fractures is optimized and improved.

2. Critical Condition for No Rolling of Proppant under Injection

Most scholars at home and abroad focus on the research and analysis on proppant backflow during fracturing but there are few studies on proppant backflow caused by gas flowing down at high speed in gas storage. On the one hand, when the gas is injected and produced in the gas storage, the high-speed flow of the gas in the gas storage causes the proppant, which was in a stable state, to be rolled and carried to the wellbore. Alternate changes in pore pressure lead to changes in effective stress, resulting in particle migration in the reservoir, resulting in sand production. This article analyzes the migration of proppant particles caused by gas flow during gas storage injection and production, which can provide reference value for gas storage to improve gas production efficiency.

Model assumptions are as follows:

(1) The supporting seam is a vertical seam, and the height and width of the seam are constant.

(2) Fracture flow is gas-liquid two-phase linear flow.

(3) The size of proppant particles is uniform, and the particles are in point contact, regardless of the deformation of the proppant.

(4) Compared with other parameters, proppant gravity has little effect on backflow, and gravity parameters are not considered in this article.

The proppant primarily supports the pressure-opened fracture, preventing it from closing and providing access for gas injection and recovery. In the construction of gas storage using depleted gas wells, when proppant fractures reach a stable state before gas injection, the force analysis of proppant is shown in Figure 1.

On the one hand, as the gas flows down the fracture from the formation, a pressure gradient is formed in the fracture, and this pressure gradient creates a drag force on the proppant propping up the fracture in the direction of the gas flow. On the other hand, in the process of fracturing, the residual fracturing fluid, the formation water, and the formation itself are attached to the surface of the proppant particles by liquid film droplets to produce capillary resistance to the flow of natural gas in the fracture, and the capillary force reacts on the solid particles and becomes the proppant reflux power.

Therefore, the critical condition for proppant backflow is

$$P_{\text{drag}} + \sigma_c' < f_n, \tag{1}$$

where $\mathbf{P_{drag}}$ is the drag force of gas, σ_c' is the equivalent capillary force strength, and $\mathbf{f_n}$ is the strength of static friction force.

2.1. Force Analysis of Proppant Particles

(1) Drag force of gas is

$$P_{\text{drag}} = -\frac{d_p}{3} \cdot \frac{dP}{dx}, \tag{2}$$

where $\mathbf{d_p}$ is the proppant diameter, m.

(2) Strength of static friction force $\mathbf{f_n}$ is

$$f_n = \mu P_c, \tag{3}$$

where $\mathbf{f_n}$ is the static friction force, μ is the static friction coefficient, and $\mathbf{P_c}$ is the closing stress.

(3) Equivalent capillary force σ_c' strength is

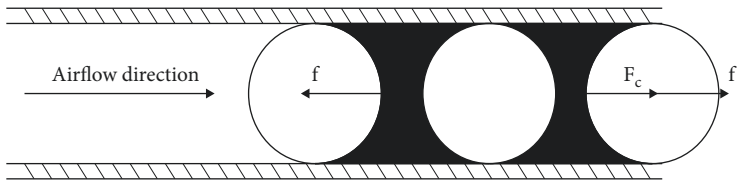

Figure 1: Schematic diagram of proppant stress.

$$\sigma_c' = \frac{2(1-\varphi)}{\varphi}\frac{\pi\sigma\sin\alpha_c^2}{d_p}\left(\frac{1}{f_1(\alpha_c)} - \frac{1}{f(\alpha_c)}\right). \quad (4)$$

During the production process of fracturing gas wells, the change of stress state and the deduced effective stress principle [23, 24] provide a reference for this article. When the fluid breaks through the capillary force, proppant particles are initiated by forces and drag forces that are consistent with the direction of flow, as seen from the action and reaction forces. This force is called the equivalent capillary force.

2.2. Critical Velocity at Which Proppant Cannot Be Transported. From the previous analysis, the mechanical conditions expressed in (1) must be satisfied for the proppant to backflow. The critical condition for proppant backflow is

$$P_{dr\,ag} + \sigma_c' = f_n. \quad (5)$$

Substitute Equations (2), (3), and (4) in (5) to obtain

$$-\frac{d_p}{3}\cdot\frac{dP}{dx} + \frac{2(1-\varphi)}{\varphi}\frac{\pi\sigma\sin\alpha_c^2}{d_p}\left(\frac{1}{f_1(\alpha_c)} - \frac{1}{f(\alpha_c)}\right) = \mu P_c. \quad (6)$$

According to the non-Darcy flow model of gas,

$$-\frac{dP}{dx} = \frac{R\mu_{gi}ZT_i\rho_a}{29P_{wf}k_g(1-S_{wi})}v + \frac{RZT_i\beta\gamma_g\rho_a^2}{29P_{wf}}v^2. \quad (7)$$

Among them, $\beta = 5.5\times10^9/k^{1.25}\varphi^{0.75}$ where K is the permeability, φ is the porosity, **Z** is the natural gas deviation factor, dimensionless, R is the dimensionless Pratt constant of gas, $\mathbf{T_i}$ is the formation temperature, **K**; $\mu_{\mathbf{gi}}$ is the viscosity of natural gas in the formation, **MPa · s**; $\rho_{\mathbf{a}}$ is the air density, $\mathbf{kg/m^3}$, $\gamma_{\mathbf{g}}$ is the relative density of natural gas, dimensionless, $\mathbf{P_{wf}}$ is the bottomhole flow pressure, **MPa**, $\mathbf{k_g}$ is the absolute fracture permeability, $\mu\mathbf{m}^2$, β is the inertial resistance coefficient, $1/\mathbf{m}$, and **v** is the gas velocity, **m/s**.The negative sign indicates that the direction of the fluid velocity is opposite to the direction of the pressure gradient.

Substituting (7) in Equation (6), a quadratic equation with one variable about gas velocity **v** is obtained:

$$\frac{R\mu_{gi}ZT_i\rho_a d_p}{87P_{wf}k_g(1-S_{wi})}v + \frac{RZT_i\beta\gamma_g\rho_a^2 d_p}{87P_{wf}}v^2 + \frac{2(1-\varphi)}{\varphi}\frac{\pi\sigma\sin\alpha_c^2}{d_p}\left(\frac{1}{f_1(\alpha_c)} - \frac{1}{f(\alpha_c)}\right) - \mu P_c = 0. \quad (8)$$

Make $A = RZT_i\beta\gamma_g\rho_a^2 d_p/87P_{wf}$,

$$B = \frac{R\mu_{gi}ZT_i\rho_a d_p}{87P_{wf}k_g(1-S_{wi})},$$

$$C = \frac{2(1-\varphi)}{\varphi}\frac{\pi\sigma\sin\alpha_c^2}{d_p}\left(\frac{1}{f_1(\alpha_c)} - \frac{1}{f(\alpha_c)}\right) - \mu P_c. \quad (9)$$

Formula (8) can be simplified into

$$Av^2 + Bv + C = 0. \quad (10)$$

The critical flow rate of proppant that does not start is

$$v = \frac{-B + \sqrt{B^2 + 4AC}}{2A}. \quad (11)$$

If the flow velocity is less than the proppant critical flow rate, the proppant in the pressure fracture will remain static. The width of the fracture is assumed to be ω_f and the height of the fracture h. According to the flow characteristics in the fracture, as long as the sand particles along the wall are not pushed, the sand particles throughout the fracture will not be pushed. For this reason, when considering the flow rate, take the velocity of the fracture in the wellbore wall as the standard and assume that all gas flows into the wellbore through the fracture. So, the production of the gas well is

$$Q = \frac{2\omega_f hv86400}{B_g}, \quad (12)$$

where ω_f is the width of the fracture; h is the height of the propped fracture, m; B_g is the volume coefficient of natural gas, m^3; and Q is the natural gas production, m^3/d.

Substitute the critical velocity in (11) to obtain the critical flow.

3. Critical Conditions under Which Proppant Is Not Discharged under Recovery Conditions

The critical condition of proppant rolling start was obtained by force analysis of proppant particles in the gas production channel, and then the law of proppant migration was analyzed.

3.1. Force Analysis of a Single Stationary Proppant Particle. It is assumed that the proppant particles in the gas production channel are spherical, and the packing mode is shown in Figure 2. The proppant particle radius is set as r, and the static proppant particles in the fluid are mainly subjected to pressure gradient force, gas impact force, and the gravity of the proppant particles themselves.

(1) Pressure gradient force F_P is

$$F_P = \frac{4}{3}\pi r^3 \left(\frac{R\mu_{gi} Z T_i \rho_a}{29 P_{wf} k_g (1 - S_{wi})} v + \frac{R Z T_i \beta \gamma_g \rho_a^2}{29 P_{wf}} v^2 \right). \tag{13}$$

(2) Gravity F_G is

$$F_G = \frac{4}{3}\pi r^3 \left(\rho_s - \frac{28.97 \gamma_g P}{RTZ} \right) g. \tag{14}$$

3.2. Rolling Starting Conditions of Proppant Particles. In the case of contact point A, the pressure gradient force and the impact force of the gas cause the proppant to roll around A, while the gravity hinders the proppant particle rolling. The moment generated by the interaction force between proppant particles 2 (see the right picture) through point A is zero, and the force generated by proppant particles 1 plays a main role in its rolling. When the proppant particles and proppant particles 1 just get out of contact, the force is zero, and the proppant particles start rolling. According to the principle of torque balance, when the active torque is greater than the retarded torque, the proppant particles will roll. That is,

$$F_P L_y \geq F_G L_x, \tag{15}$$

where L_x and L_y are the hindrance moment arm and the main force moment arm, respectively. Its moment arm can be obtained from geometric relations.

When the gas flow rate meets (15), proppant particles will roll. Substitute the above force expressions (13) and (14) in Equation (15) to obtain the following:

$$\left[\frac{4}{3}\pi r^3 \left(\frac{R\mu_{gi} Z T_i \rho_a}{29 P_{wf} K_g (1 - S_{wi})} \right) v + \frac{R Z T_i \beta r_g \rho_a^2}{29 P_{wf}} v^2 \right] \frac{\sqrt{3}}{2} r \geq \left[\frac{4}{3}\pi r^3 \left(\rho_s - \frac{28.97 K_g P}{RTZ} \right) g \right] \frac{r}{2}. \tag{16}$$

Similarly, a quadratic equation with one variable about gas velocity v is obtained:

$$\frac{R\mu_{gi} Z T_i \rho_a}{29 P_{wf} k_g (1 - S_{wi})} v + \frac{R Z T_i \beta \gamma_g \rho_a^2}{29 P_{wf}} v^2 + \frac{\sqrt{3}}{3} \left(\frac{28.97 \gamma_g P}{RTZ} - \rho_s \right) \geq 0. \tag{17}$$

Make $A_1 = RZT_i \beta \gamma_g \rho_a^2 / 29 P_{wf}$,

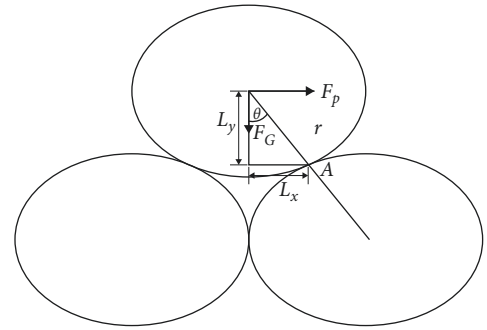

Figure 2: Analysis of proppant stress during gas recovery.

$$B_1 = \frac{R\mu_{gi} Z T_i \rho_a}{29 P_{wf} k_g (1 - S_{wi})}, \quad C_1 = \frac{\sqrt{3}}{3} \left(\frac{28.97 \gamma_g P}{RTZ} - \rho_s \right). \tag{18}$$

Formula (18) can be simplified into

$$A_1 v^2 + B_1 v + C_1 \geq 0. \tag{19}$$

Therefore, the proppant velocity of the produced gas should meet the following requirements:

$$v \geq \frac{-B_1 + \sqrt{B_1^2 + 4A_1 C_1}}{2A_1}. \tag{20}$$

Therefore, the critical velocity of proppant particle rolling is

$$v_g = \frac{-B_1 + \sqrt{B_1^2 + 4A_1 C_1}}{2A_1}. \tag{21}$$

3.3. Rolling Start-Up Conditions under Different Proppant Arrangements. In the actual gas production channel, proppant particles are not necessarily arranged in the gas production channel as shown in Figure 2, some proppant grains may be submerged, and some may be embedded in other grains. The grain arrangement after the gas production channel has the following three forms as shown in Figure 4, and the distance from the contact point of proppant grains to the lower boundary of proppant grains is defined as the coverage depth h_r.

The proppant particles are spherical particles with equal particle size, and the coverage depth can be calculated based on the geometric relationship. In the proppant arrangement, the particle size of the proppant particles is assumed to be ds, and the distance between the center of the next two particles is $ds + \delta$, where $0 \leq \delta \leq ds$:

$$h_r = \frac{d_s - \sqrt{d_s^2 - (d_s + \delta/2)^2}}{2}. \tag{22}$$

When $\delta = 0$, the proppant is arranged in the form shown in Figure 4(a), and the minimum coverage depth of proppant particles is $h_r = 0.067\ ds$.When $\delta = ds$, the proppant is

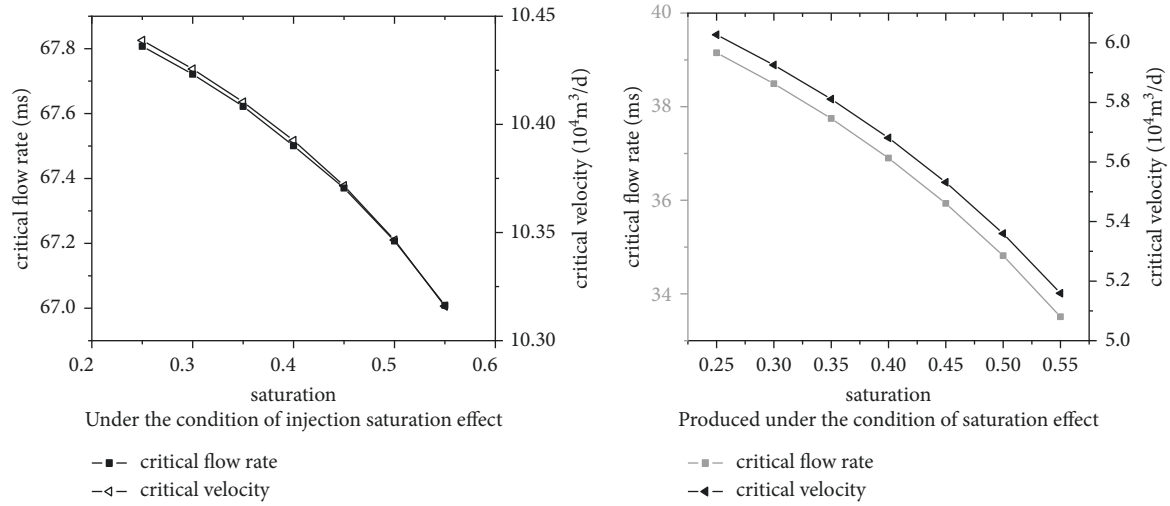

Figure 3: Influence diagram of saturation under injection-production conditions.

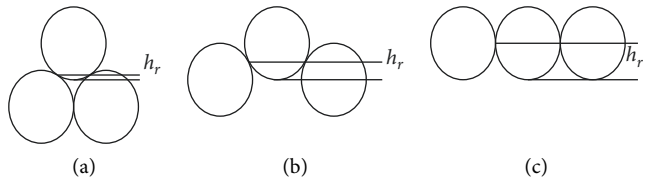

Figure 4: Schematic diagram of proppant arrangement during gas recovery.

arranged in the form shown in Figure 4(c), and the maximum coverage depth of proppant particles is $h_r = 0.5\ ds$.

Different proppant particle coverage will affect the moment arms of each force when the particle rolling starts. After considering the proppant particle coverage, the moment arms of each force are

$$l_x = \frac{d_s + \delta}{4} = \sqrt{d_s h_r - h_r^2}, l_y = \frac{\sqrt{d_s^2 - ((d_s + \delta)/2)^2}}{2} = \frac{d_s}{2} - h_r. \tag{23}$$

By substituting the force arm formula (23) into formula (21), the critical rolling velocity of proppant particles considering the arrangement of proppant can be obtained. In addition, the critical rolling velocity considering the arrangement of proppant particles and the shape of proppant particles can be obtained by combining the equivalent particle size formula of different proppant shapes.

Substitute the critical velocity in (12) to obtain the critical flow formula as follows:

$$Q_{qc} = \frac{2w_f h v_g 86400}{B_g}. \tag{24}$$

Thus, as long as the production rate of the gas well is less than Q_{qc}, the gas well will not destroy the supporting sand in the fracture, so that the fracture can maintain long-term effectiveness.

4. Calculation Model of Proppant Migration Fluid Velocity

When the proppant is sheared or stretched by the fluid, the proppant particles fall off from the surface of the rock skeleton. After the particles fall off, the force of the proppant in the pore fluid is different under different fluid conditions, which determines whether the proppant particles can be taken away by the fluid or remain in place after falling off from the surface of the rock skeleton. The research of scholars in other fields can provide us with some references. [26–28] When proppant particles migrate, deposit, and plug in pores, they will cause changes in reservoir physical parameters, especially porosity and permeability, and then affect reservoir productivity.

Before the reservoir rock is deformed, its original porosity is

$$\varphi_0 = \frac{V_p}{V_f} = \frac{V_f - V_r}{V_f}, \tag{25}$$

where V_f is the total volume of rock, m^3, V_p is the pore volume, m^3, and V_r is the volume of rock skeleton, m^3.

In the stable production stage of the gas storage, the bottom hole pressure remains unchanged and the resulting pressure drop remains constant. The pressure at any point of the gas storage can be regarded as unchanged, and the influence of pressure on it can be ignored. When most mobile proppant particles stop migration, the permeability will gradually stabilize.

Then, the porosity of proppant after being carried out of gas storage by liquid is

$$\varphi = \varphi_0 + (1 - \varphi_0)\frac{R_c}{\rho_s}. \tag{26}$$

Seepage velocity is

$$v_s = \frac{14.4W}{A\varphi}. \tag{27}$$

Substitute equation (26) in

$$v_s = \frac{14.4W}{A[\varphi_0 + (1 - \varphi_0)R_c/\rho_s]}, \tag{28}$$

where W is the liquid volume flow. The above formula is the velocity of proppant migration.

The determination of proppant carrying fluid velocity aims at improving the single well production of gas storage wells, and the single well production formula is

$$Q = \frac{kh\Delta p}{141^2\mu\beta\left(p_j + s\right)}, \tag{29}$$

where Q is the gas production, k is the reservoir permeability, h is the reservoir thickness, β is the fluid volume coefficient, s is the skin coefficient of wellbore, and p_j is the desorption pressure at point j.

When the liquid flows slowly in the gas production channel, proppant particles may deposit and block in the channel. When the fluid velocity is too high, it may scour the gas production channel wall, which may cause a large number of proppant particles to discharge and close the crack. In order to prevent deposition, wall scouring, and proppant discharge in the gas production channel, the fluid velocity should not be too large or too small. Under the condition of ensuring the maximum permeability, selecting an appropriate flow rate can improve the production of gas storage and gas production efficiency. Accordingly, the flow rate should be the following:

Under injection conditions: $v_i \ll v_{D1} \ll v_s$

Under recovery conditions: $v_g \ll v_{D2} \ll v_s$

By comparing with the production data of 20 wells in the gas storage in the Yulin gas field, critical velocity, critical flow, and fluid flow range all verify the rationality of the calculation results in this article.

5. Sensitivity Analysis of Influencing Factors

5.1. Basic Parameters. The southwest reservoir of Yulin gas field gas storage has a buried depth of 2850 ~ 3100 m, a formation temperature of 90°C, and a storage capacity of $177.62 \times 108\ m^3$, an average thickness of 10.1 m, and a porosity of 4.1 ~ 8.3%, and the average porosity is 6.4%. The permeability is 0.1 ~ 20.3 mD, belonging to low porosity and low permeability gas reservoir. The basic parameters calculated by the model are as follows: formation pressure of 27.7 MPa, reservoir temperature of 364°C, air density of 1.3 kg/m^3, natural gas volume coefficient of 0.0041, natural gas relative density of 0.625 kg/m^3, natural gas viscosity of 0.02 MPa·s, proppant of 20/40 mesh, deviation factor of 0.78, gas proctor constant of 8.314, relative density of 3.34 kg/m^3, and proppant apparent density of 2.2 g·m^{-3}. The bulk density of proppant is 1.59 g m^{-3}, the strength of proppant is 20.7–34.5 MPa, the internal friction angle is 30°, and the uniaxial compressive strength is 12 MPa.

5.2. Crack Width. It can be seen from Figure 5 that with the increase in the width of the supporting crack, the critical air velocity gradually decreases, the filling layer is more unstable, and the proppant is prone to backflow. On the contrary, the smaller the fracture width, the higher the critical air velocity, the more stable the filling layer, and the more difficult it is to reflow.

The wider the supporting fracture is, the easier the backflow is, but the higher the critical production of the gas well is. On the contrary, the narrower the supporting fracture is, the less likely the backflow is, but the lower the critical production of the gas well is. In other words, there is a certain contradiction between proppant backflow prevention and gas well production. We must find an optimal fracture width to reconcile the contradiction between the two and achieve optimization.

5.3. Closure Stress. As shown in Figure 6, the greater the closure stress, the more stable the proppant filling layer, and the greater the critical flow rate of reflux. The closure stress is equal to the formation pressure minus the pore pressure. With the continuous production of natural gas, the pore pressure decreases and the closure stress increases gradually.

As the closure stress increases, the critical flow rate and critical velocity of proppant reflux gradually increase, and the proppant filling layer becomes more stable. There is an obvious linear relationship between the critical flow rate and the closure stress.

5.4. Saturation. As shown in Figure 3, the influence of water irreducible saturation on the stability of the filling layer is very obvious. The smaller the S_w is, the greater the critical air velocity is, and the more stable the filling layer is. On the contrary, the larger the S_w is, the lower the critical gas velocity is, and the more likely the proppant is to reflux.

At the initial stage of gas storage well production, S_w is large, the fracture flow is gas-liquid two-phase flow, and the pressure gradient is large. At this time, the supporting fracture is the most unstable, so the gas well production should not be too high. With the flow of natural gas, the working fluid flows out together, and the stability of supporting fractures is enhanced, which can appropriately increase the production of gas wells.

5.5. Production Differential Pressure. The greater the production pressure difference, the lower the critical velocity of proppant backflow, the more unstable the support crack, and the proppant backflow is easy to occur.

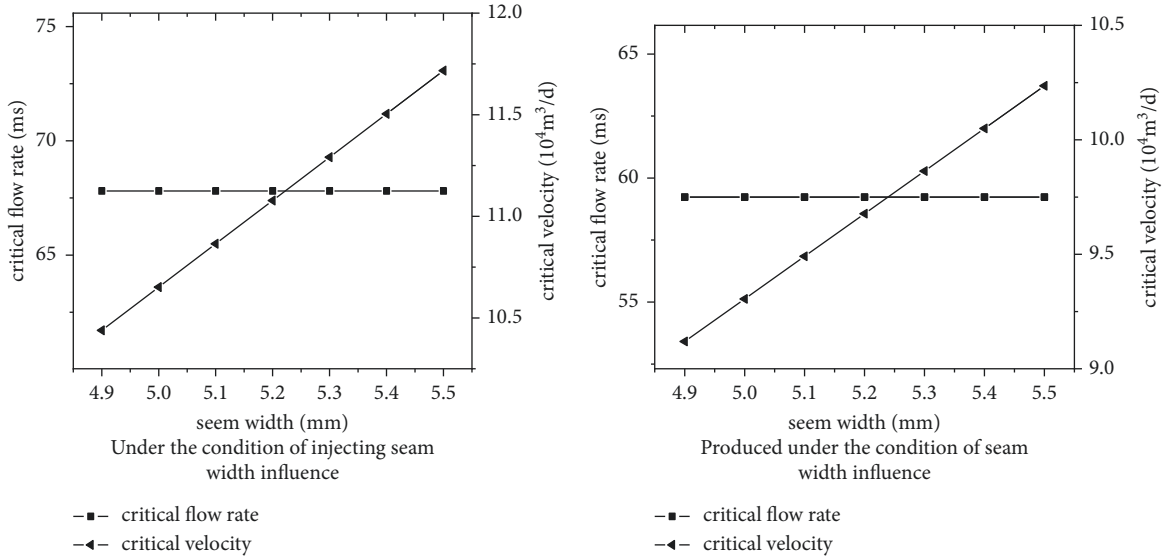

Figure 5: Influence diagram of fracture width under injection-production conditions.

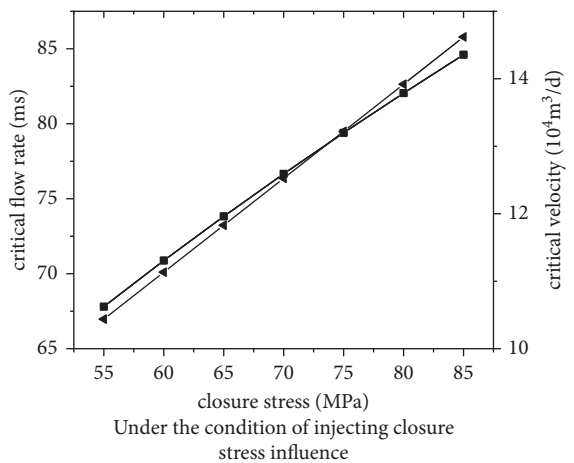

Figure 6: Influence diagram of closure stress under injection condition.

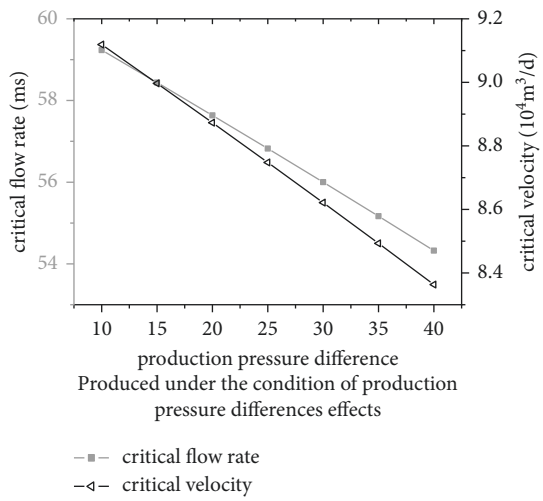

Figure 7: Influence diagram of production pressure difference under production conditions.

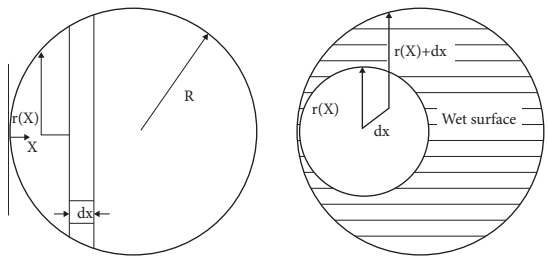

Figure 8: Schematic diagram of the calculation model of drag force.

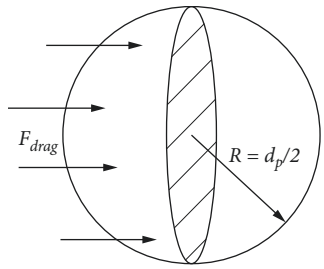

Figure 9: Schematic diagram of proppant stress.

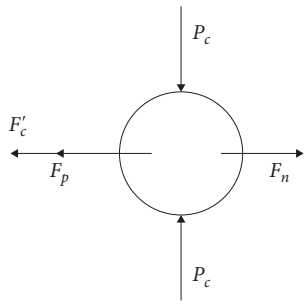

Figure 10: Analysis of proppant stress during gas injection.

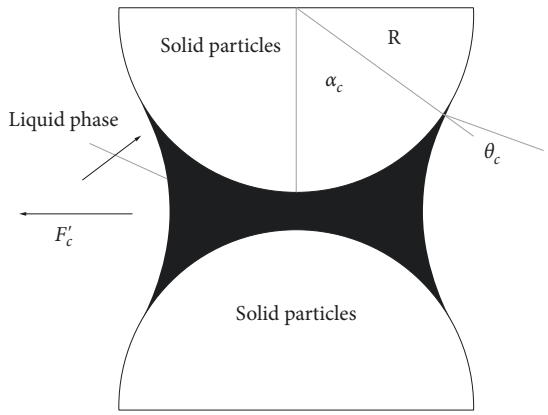

Figure 11: Schematic diagram of capillary force action.

As shown in Figure 7, with the increase in production differential pressure, the production of gas wells increases. However, the greater the differential pressure, the lower the critical flow rate and production of proppant backflow in gas wells. In other words, if the production pressure difference is too large, it is easy to cause proppant backflow, resulting in the reduction of fracture conductivity.

6. Conclusion

(1) When the supporting fracture reaches a stable state in the process of gas injection and production, the range between the critical velocity of backflow and the velocity of proppant migration is determined through the force analysis of proppant, and the maximum permeability of the reservoir is determined, which can improve the gas production efficiency to the greatest extent.

(2) When the proppant is no longer in a stable state, the proppant migrates, which will have a certain impact on the porosity and permeability of the gas production channel. Moderately discharging a certain amount of separated proppant particles can increase the gas production efficiency and improve the gas production.

(3) With the increase of closure stress, the critical gas flow and critical gas velocity of proppant backflow gradually increase, and the proppant filling layer is more stable. The critical flow rate and critical flow measured at the closure stress point have an obvious linear relationship with the closure stress, which has a strong regularity.

(4) The smaller the thickness of the filling layer is, the greater the critical gas flow and critical gas velocity of proppant backflow, the more stable the proppant filling layer is, and the chance of backflow is reduced. There is a consistent relationship between the critical velocity and critical flow and the fracture width.

(5) The influence of irreducible water saturation on the stability of the filling layer is very obvious; the greater the production differential pressure, the lower the critical velocity of proppant backflow, and the more unstable the support fracture, which is prone to proppant backflow. The production differential pressure should be controlled within a reasonable range during gas well production.

Appendix

A. Critical Condition for No Rolling of Proppant under Injection Part Formula Derivation

Force analysis of proppant particles

(1) Drag Force of Gas. In the actual production process of a gas well, the high-speed flow of gas in the proppant fracture is linear non-Darcy two-phase flow, and the pressure changes along the fracture length with a parabola. For uniform pressure gradient, the flow pressure changes linearly with distance, and then

$$P(x) = P_0 + \frac{dP}{dx}x, \tag{A.1}$$

where the $P(x)$ is the fluid pressure, P_0 is the uniform pressure gradient , and x is the strength.

When calculating the drag force acting on a single proppant, the gas-liquid two-phase flow in the propped fracture is considered. For both gas-phase flow and liquid-phase flow, the total pressure drop of the entire joint length is assumed to be **dP/dx**, and the fluid pressure drop produces drag force. The wet phase surface is projected on the plane normal of the flow direction, as shown in Figure 8.

A segment of microelement distance **dx** on a single proppant particle is taken, and the drag force acting on this segment is

$$dF_{\mathrm{drag}(x)} = P(x)dA_{wp}, \tag{A.2}$$

where $F_{\mathrm{drag}(x)}$ is the drag force at the distance between the proppant particles; A_{wp} is the P(x) applied to the area at the distance between proppant particles, m^2; and P(x) is the pressure, MPa

The unit stressed area on the proppant particle at x is

$$dA_{wp} = 2\pi r(x)dr. \tag{A.3}$$

Substituting Equations (A.1) and (A.3) in Equation (A.2), we can get

$$dF_{\mathrm{drag}(x)} = \left(P_0 + \frac{dP}{dx}x\right)2\pi r(x)dr. \tag{A.4}$$

Equation (A.4) describes the drag force acting on a segment of the proppant particle. The total drag force acting on the entire proppant particle can be viewed as a proppant particle composed of an infinite number of such segments:

$$F_{\mathrm{drag}} = 2\pi P_0 \int_0^{2R} (R - x)\mathrm{d}x + 2\pi \frac{dP}{dx} \int_0^{2R} x(R - x)\mathrm{d}x. \tag{A.5}$$

Integrate Equation (A.5) to obtain

$$F_{\mathrm{drag}} = -\frac{4}{3}\pi \frac{dP}{dx}R^3. \tag{A.6}$$

As the fluid flows through the propped fracture, the flow pressure drop generates a drag force, the action of which is shown in Figure 9.

The drag force $\mathbf{F_{drag}}$ is applied to the shaded area shown in the figure. It can be seen from the figure that the stressed area $\mathbf{A_p}$ is half of the spherical area of proppant particles, $\mathbf{A_p} = 2\pi\mathbf{R}^2$. The intensity of drag force acting on $\mathbf{A_p}$ is

$$P_{\mathrm{drag}} = \frac{F_{\mathrm{drag}}}{2\pi R^2}, \tag{A.7}$$

where $\mathbf{P_{drag}}$ is the strength of drag force, **MPa**.

Substituting Equation (A.6) in Equation (A.7), we can get [18]

$$P_{\mathrm{drag}} = -\frac{2R}{3} \cdot \frac{dP}{dx}. \tag{A.8}$$

If the diameter of proppant particle is $\mathbf{d_p}$, then $\mathbf{R} = \mathbf{d_p}/2$ is substituted into Equation (A.8) to obtain

$$P_{\mathrm{drag}} = -\frac{d_p}{3} \cdot \frac{dP}{dx}, \tag{A.9}$$

where $\mathbf{d_p}$ is the proppant diameter, *m*.

(2) Strength of Static Friction Force $\mathbf{f_n}$. The value of static friction force is proportional to the product of closing pressure, particle contact area, and static friction coefficient. The larger the closing pressure, the larger the particle contact area, the rougher the particle surface, and the greater the static friction force. The less likely the proppant is to start (Figure 10).

The maximum static friction force can be expressed as

$$f_n = \mu P_c, \tag{A.10}$$

where $\mathbf{f_n}$ is the static friction force, μ is the static friction coefficient, and $\mathbf{P_c}$ is the closing stress.

(3) Equivalent Capillary Force σ_c' *Strength*. During the production process of fractured gas wells, there are multi-phase fluids in fractures, including working fluid residual in fractures and formation fluid. The flow in fractures is gas-liquid two-phase. With the flow of natural gas, capillary resistance occurs, and the direction is opposite to the flow direction of the fluid, hindering the flow of the fluid. When the fluid breaks through the capillary force, it can be seen from the acting and reaction forces that the proppant particles are started by a force consistent with the flow direction and a drag force. This force is called the equivalent capillary force, which is equal to the capillary force and opposite to the capillary force, as shown in Figure 11.

Assuming that the proppant particle size is uniform, tangential contact capillary force of particles with uniform size can be expressed as

$$F_C' = \frac{1}{2}\pi\sigma d_p \sin\alpha_c^2 \left(\frac{1}{f_1(\alpha_c)} - \frac{1}{f(\alpha_c)}\right). \tag{A.11}$$

Among them,

$$f_1(a_c) = \left\{\frac{1}{\cos a_c}\left[\sin a_c \cos a_c + (1 - \cos a_c)(\sin(\theta_c + a_c) - 1)\right]\right\},$$
$$\cdot f(a_c) = \frac{1 - \cos a_c}{\cos a_c}, \tag{A.12}$$

where θ_c is the contact angle, α_c is the angle between the radius of the solid-liquid boundary on the proppant particle and the vertical axis, σ is the interfacial tension between fluids, N/m, and $\mathbf{d_p}$ is the diameter of the proppant. Since there is no difference in particle size, the capillary force strength in tangential contact of particles can be expressed as

$$\sigma_c' = \frac{1 - \phi}{\phi} \frac{\pi\sigma \sin\alpha_c^2}{R} \left(\frac{1}{f_1(\alpha_c)} - \frac{1}{f(\alpha_c)}\right), \tag{A.13}$$

where $\mathbf{d_p}$ is the diameter of proppant, so $\mathbf{R} = \mathbf{d_p}/2$. Put in the above equation to obtain the following:

$$\sigma_c' = \frac{2(1-\varphi)}{\varphi}\frac{\pi\sigma \sin \alpha_c^2}{d_p}\left(\frac{1}{f_1(\alpha_c)} - \frac{1}{f(\alpha_c)}\right). \quad (A.14)$$

B. Critical Conditions under Which Proppant Is Not Discharged under Recovery Conditions Part Formula Derivation

(1) Pressure Gradient Force F_p. The fluid flows under the action of pressure gradient, within which the force on the surface of proppant particles is different, and the resultant force on the surface is the pressure gradient force of proppant particles, which can be expressed as

$$F_p = 2\pi r^2 \int_0^{\pi}\left(P_0 + r(1+\cos\theta)\frac{\partial P}{\partial x}\right)\cos\theta \sin\theta \, d\theta = \frac{4}{3}\pi r^3 \frac{\partial P}{\partial x}, \quad (B.1)$$

where r is the radius of the proppant particle, $\partial P/\partial x$ is the pressure gradient, and its direction is consistent with the movement direction of the proppant particle.

Under a certain pressure gradient, the liquid will flow. According to the non-Darcy seepage formula, it can be seen that

$$-\frac{dP}{dx} = \frac{R\mu_{gi}ZT_i\rho_a}{29P_{wf}k_g(1-S_{wi})}v + \frac{RZT_i\beta\gamma_g\rho_a^2}{29P_{wf}}v^2. \quad (B.2)$$

Substitute the above equation in Equation (B.2), and the force generated by the pressure gradient can be expressed by fluid velocity as follows:

$$F_P = \frac{4}{3}\pi r^3\left(\frac{R\mu_{gi}ZT_i\rho_a}{29P_{wf}k_g(1-S_{wi})}v + \frac{RZT_i\beta\gamma_g\rho_a^2}{29P_{wf}}v^2\right). \quad (B.3)$$

(2) Gravity F_G. The gravity of proppant particles in the gas is the gravity after considering the buoyancy force, and its relationship is

$$F_G = \frac{4}{3}\pi r^3(\rho_s - \rho_q)g, \quad (B.4)$$

where ρ_s is the density of proppant and ρ_q is the density of gas. The gas density $\rho_q = 28.97\gamma_g P/RTZ$ is substituted in equation (B.4):

$$F_G = \frac{4}{3}\pi r^3\left(\rho_s - \frac{28.97\gamma_g P}{RTZ}\right)g. \quad (B.5)$$

C. Calculation Model of Proppant Migration Fluid Velocity Part Formula Derivation

Before the reservoir rock is deformed, its original porosity is

$$\varphi_0 = \frac{V_p}{V_f} = \frac{V_f - V_r}{V_f}, \quad (C.1)$$

where V_f is the total volume of rock, m^3, and V_p is the pore volume,m^3, and V_r is the volume of rock skeleton, m^3.

(1) Effect of Pressure Change. In the process of gas storage injection and production, when the formation conditions change from initial state (P_0, t_0) to state (P, t_0), the volumetric strain coefficient of rock in this process is ε_v. Then, the total volume change of rock is

$$\Delta V_f = V_f\varepsilon_v. \quad (C.2)$$

(2) Influence of Proppant Separation, Deposition, and Blockage. The separation of proppant, deposition on pore surface, and blockage in throat are attributed to the change of rock skeleton volume, which makes the skeleton volume decrease to negative and increase to positive. Therefore, the change of rock skeleton volume can be expressed as

$$\Delta V_s = V_r\left(-\frac{R_r}{\rho_s} + \frac{R_d}{\rho_s} + \frac{R_p}{\rho_s}\right), \quad (C.3)$$

where R_r is the mass separation amount of skeleton proppant on unit volume rock, kg/m^3 ; R_d is the mass deposition of proppant on the pore surface per unit volume of rock, kg/m^3 ; R_p is the mass retention of proppant in pore throat blockage on unit volume rock, kg/m^3.

R_r is determined by the skeleton stripping constitutive equation as follows:

$$R_r = \rho_s\lambda(1-\varphi_0)C_s q^{0.5}, \quad (C.4)$$

where λ is the liquefaction coefficient of rock, which is determined by experimental test; q is the volume of fluid and proppant mixture flowing through unit area in unit time; and C_s is the volume concentration of proppant.

R_d is determined by the pore surface deposition equation as follows:

$$R_d = \begin{cases} K_{d1}vC_s\rho_s, \\ K_{d1}vC_s\rho_s - K_{d2}R_d(v - v_{g1j}), \end{cases} \quad (C.5)$$

where K_{d1} and K_{d2} are surface deposition rate constants.

$$R_p = K_p V C_s \rho_s, \quad (C.6)$$

where K_p is the pore throat plugging rate constant. When $t = 0$, $R_p = 0$, so the porosity of rock under pressure and after proppant separation, deposition, and plugging at pore throat is

$$\varphi = \frac{(V_f + \Delta V_f) - (V_r + \Delta V_s)}{V_f + \Delta V_f}. \quad (C.7)$$

Substitute equation (C.1) and equation (C.2) into equation (C.7):

$$\varphi = 1 - \frac{1-\varphi_0}{1+\varepsilon_v}\left(1 - \frac{R_r - R_d - R_p}{\rho_s}\right). \quad (C.8)$$

$R_c = R_r - R_d - R_p$ where R_c is the discharge amount of particles per unit volume of rock with liquid, kg/m^3. Then, the porosity after proppant is carried out of the reservoir by liquid is

$$\varphi = 1 - \frac{1-\varphi_0}{1+\varepsilon_v}\left(1 - \frac{R_c}{\rho_s}\right). \quad (C.9)$$

In the stable production stage of the gas storage, the bottom hole pressure remains unchanged and the resulting pressure drop remains constant. The pressure at any point of the gas storage can be regarded as unchanged, and the influence of pressure on it can be ignored. When most mobile proppant particles stop migration, the permeability will gradually stabilize. Then, the porosity of proppant after being carried out of gas storage by liquid is

$$\varphi = \varphi_0 + (1-\varphi_0)\frac{R_c}{\rho_s}. \quad (C.10)$$

Data Availability

The data (data type) used to support the findings of this study are included within the article.

Conflicts of Interest

The authors declare that they have no conflicts of interest.

Acknowledgments

The experiments in this research program were supported by the key laboratory of well stability and fluid and rock mechanics in oil and gas reservoir of Shaanxi province. This research was funded by the National Natural Science Foundation of China (Grant nos. 51974255 and 51874240), the Natural Science Basic Research Program of Shaanxi (Program number: 2020JM-544), the Shaanxi Province Key Research and Development Plan (Program number: 2020KW-027), the Shaanxi Provincial Science Fund for Distinguished Young Scholars (Program number: 2022JC-37), and the Xi'an Shiyou University Graduate Innovation and Practice Ability Training Program (Project number: YCS20213149).

References

[1] C. D. Hall Jr and W. H. Harrisberger, "Stability of sand arches: a key to sand control," *Journal of Petroleum Technology*, vol. 22, no. 7, pp. 821–829, 1970.

[2] R. K. Bratli and R. Risnes, "Stability and failure of sand arches," *Society of Petroleum Engineers Journal*, vol. 21, no. 2, pp. 236–248, 1981.

[3] M. Tayler, C. Stephenson, and M. I. Asgian, "Factors affecting the stability of proppant in propped fractures: results of a laboratory study," in *Proceedings of the SPE Annual Technical Conference and Exhibition*, WashingtonDC, October 1992.

[4] J. L. Gidley, G. S. Penny, and R. R. McDaniel, "Effect of proppant failure and fines migration on conductivity of propped fractures," *SPE Production and Facilities*, vol. 10, no. 1, pp. 20–25, 1995.

[5] N. Goel and N. S. Subhash, "Experimental investigation of proppant flow back phenomena using a large scale fracturing simulation," vol. 10, 1999.

[6] J. Romero and J. P. Feraud, "Stability of proppant pack reinforced with fiber for proppant flow back control," *Society of Petroleum Engineers Journal*, no. 2, pp. 231–237, 1996.

[7] M. Javier, "Avoiding proppant flow back in tight-gas completions with improved fracture design," vol. 10, 2003.

[8] T. Esmaeel Kazemi, J. Arezou, and T. Ali, "Gas-water-rock interactions and factors affecting gas storage capacity during natural gas storage in a low permeability aquifer," *Petroleum Exploration and Development*, vol. 45, no. 6, pp. 1123–1128, 2018.

[9] Z. Qu, Q. Lin, T. Guo, and Y. Wang, "Experimental study on conductivity of carbonate acid etched fractures in Shunbei Oilfield," *Fault-Block Oil & Gas Field*, vol. 26, no. 4, pp. 533–536, 2019.

[10] M. Cesar, "Cerda. Mobilization of quartz fines in porous media," *Clays and Clay Minerals*, vol. 36, no. 6, 1988.

[11] H. Reza, P. Peyman, V. Ali, and S. Abdolhamid, "Application of silica nanofluid to control initiation of fines migration," *Petroleum Exploration and Development Online*, vol. 44, no. 5, 2017.

[12] Q. Chen, "Quantitative calculation method of particle transport critical velocity and damage radius," *Petroleum Geology and Engineering*, vol. 30, no. 4, pp. 113-114+118, 2016.

[13] D. Chen, Z. Pan, Z. Ye, B. Hou, D. Wang, and L. Yuan, "A unified permeability and effective stress relationship for porous and fractured reservoir rocks," *Journal of Natural Gas Science and Engineering*, vol. 29, pp. 401–412, 2016.

[14] Li Yao, Y. Xie, H. Xue, and Y. Zhang, "Analysis of sand production mechanism and determination of reasonable production allocation of gas wells in Yulin gas field," *Petrochemical applications*, vol. 35, no. 11, 2016.

[15] Y. Zou, J. Guo, and C. Fu, "Study on determination method of critical sand production in fractured gas wells," *Natural gas exploration and development*, vol. 32, no. 03, 2009.

[16] T. Li, *Study on ancient fracturing theory and application technology in Yulin gas field*, Southwest Petroleum University, Chengdu City, 2009.

[17] L. Li, "Study and application of critical production model for fracture sand production in gas wells," *Petrochemical applications*, no. 04, pp. 15–17, 2005.

[18] Y. Fu, *Study on proppant backflow mechanism in fracturing gas well production*, Southwest Petroleum University, Chengdu City, 2006.

[19] G. Liu, *Study on proppant backflow and control in fracturing gas well production*, Southwest Petroleum University, Chengdu City, 2018.

[20] Z. Jin, J. Guo, J. Zhao, J. Wang, and Z. Zhao, "Dan Kuang Experimental study on the effect of proppant combination with different particle size on fracture conductivity," *Petroleum Geology and Engineering*, no. 06, pp. 88–90, 2007.

[21] L. Wang and S. Zhang, "Experimental study on the effect of backflow prevention fiber on the conductivity of proppant," *Drilling and Production Technology*, vol. 33, no. 04, 2010.

[22] Y. Kang, J. Shao, L. You et al., "Experimental simulation of particle migration induced by sharp change of gas injection

pressure in gas storage wells," *Oil drilling and production technology*, vol. 42, no. 6, pp. 797–803+810, 2020.

[23] B. Bai, Q. Nie, Y. Zhang, X. Wang, and W. Hu, "Cotransport of heavy metals and SiO2 particles at different temperatures by seepage," *Journal of Hydrology*, vol. 597, Article ID 125771, 2021.

[24] B. Bai, R. Zhou, G. Cai, W. Hu, and G. Yang, "Coupled thermo-hydro-mechanical mechanism in view of the soil particle rearrangement of granular thermodynamics," *Computers and Geotechnics*, vol. 137, no. 8, Article ID 104272, 2021.

[25] F. Zhang, *Study on damage mechanism and repair technology of gas production channel in coalbed methane well*, China University of Petroleum, China, 2013.

[26] X. Y. Wang, Z. Ma, and Y. T. Zhang, "Research on safety early warning standard of large-scale underground utility tunnel in ground fissure active period," *Frontiers of Earth Science*, vol. 10, 2022.

[27] X. Wang, Q. Song, and H. Gong, "Research on deformation law of deep foundation pit of station in core region of saturated soft loess based on monitoring," *Advances in Civil Engineering*, vol. 2022, pp. 1–16, Article ID 7848152, 2022.

[28] N. Liu, L. Cui, Y. Wang, and E. Yilmaz, "Analytical assessment of internal stress in cemented paste backfill," *Advances in Materials Science and Engineering*, vol. 2020, pp. 1–13, Article ID 6666548, 2020.